Single-cell detection by gradient echo 9.4 T MRI: a parametric study

Pierre Smirnov, Florence Gazeau, Jean-Claude Beloeil, Bich-Thuy Doan, Brigitte Gillet, Claire Wilhelm

CONTRAST MEDIA & MOLECULAR IMAGING
Contrast Med. Mol. Imaging **1**: 165–174 (2006)
Published online in Wiley InterScience (www.interscience.wiley.com). DOI:10.1002/cmmi.104

CONTRAST MEDIA & MOLECULAR IMAGING

Full Paper

Single-cell detection by gradient echo 9.4 T MRI: a parametric study

P. Smirnov[1], F. Gazeau[1], J.-C. Beloeil[2], B.T. Doan[2], C. Wilhelm[1] and B. Gillet[3]*

[1]*Laboratoire Matière et Systèmes Complexes, Université Paris 7, Denis Diderot and CNRS UMR 7057, 140, rue de Lourmel, 75015 Paris, France*
[2]*Centre de biophysique moléculaire, †CNRS UPR 4301, rue Charles Sadron, 45071 Orléans, France*
[3]*Institut de Chimie des Substances naturelles, †CNRS UPR 2301, avenue de la Terrasse, 91198 Gif sur Yvette, France*

Received 22 May 2006; Revised 28 June 2006; Accepted 9 July 2006

ABSTRACT: Recent studies have shown that cell migration can be monitored *in vivo* by magnetic resonance imaging after intracellular contrast agent incorporation. This is due to the dephasing effect on proton magnetization of the local magnetic field created by a labelled cell. Anionic iron oxide nanoparticles (AMNP) are among the most efficient and non-toxic contrast agents to be spontaneously taken up by a wide variety of cells. Here we measured the iron load and magnetization of HeLa tumour cells labelled with AMNP, as a function of the external magnetic field. High-resolution gradient echo 9.4 T MRI detected individual labelled cells, whereas spin echo sequences were poorly sensitive. We then conducted a systematic study in order to determine the gradient echo sequence parameters (echo time, cell magnetization and resolution) most suitable for *in vivo* identification of single cells. Copyright © 2006 John Wiley & Sons, Ltd.

KEYWORDS: MRI; contrast agent; iron oxide nanoparticles; cell tracking; single cell detection

INTRODUCTION

Magnetic resonance imaging is a method of choice for long-term, longitudinal and non-invasive *in vivo* tracking of injected cells, thanks to its high spatial resolution and the availability of safe contrast agents (1). Superparamagnetic iron oxide particles have been used to label a wide variety of cells, without affecting their proliferation, differentiation or other functions (2–9). Such labelled cells also maintain their therapeutic potential, showing the biocompatibility of iron oxide nanoparticles. Anionic magnetic nanoparticles (AMNP) are stabilized in colloidal suspension by negative surface charges, and are not polymer-coated, contrary to conventional iron oxide nanoparticles. These negative surface charges create a high affinity for cell membranes, through electrostatic interactions. Once adsorbed to the plasma membrane, AMNP are rapidly internalized along the endocytosis pathway (10,11). These anionic nanoparticles rapidly and efficiently label most cell types, without the need for transfection agents or long incubation times (12), or for complex nanoparticle structures such as magnetodendrimers (3) or Tat-peptide-modified nanoparticles (6). We demonstrated the biocompatibility of AMNP with human gingival fibroblasts (13), lymphocytes (14) and smooth muscle cells (15). AMNP have been used as cell labels to monitor the homing of hybridomas to the spleen (16), T cells to the pancreas in autoimmune diabetes (17), T cell recruitment by tumours (14) and cardiac smooth muscle cell transplantation (15).

However, monitoring of stem cell homing (3,4,7) or T cell trafficking (5,18) may involve very small numbers of cells. For example, only a tiny fraction of injected stem cells reach their target sites. Non-invasive imaging methods capable of detecting individual cells would therefore be extremely useful.

Endosomal magnetic labelling leads to significant signal changes, as it strongly affects T_2^* and, to a lesser extent, T_2 and T_1 proton relaxation times (3,19,20). By refining the MR hardware (magnetic field intensity, detection coils, imaging pulse sequences and cell labelling modalities), some authors have detected single cells, not only *in vitro* (21–26) but also *in vivo* (27,28).

Here we examined the respective roles of various parameters (pulse sequence, cell iron load, echo time and resolution) for detection of single magnetically labelled HeLa tumour cells with a 9.4 T MRI device. Cellular iron uptake was quantified by magnetophoresis, and the magnetic moment of labelled cells was measured as a function of the external magnetic field. Gradient echo sequences were compared with spin echo sequences. The

**Correspondence to*: P. Smirnov, Laboratoire Matière et Systèmes Complexes, Université Paris 7—Denis Diderot and CNRS UMR 7057, 140, rue de Lourmel, 75015 Paris, France.
E-mail: pierre_smirnov@hotmail.com
†Member of the Network of Excellence: European Molecular Imaging Laboratories (EMIL).

influence of magnetic labelling, the echo time and the resolution of gradient echo sequences on the detection threshold was also investigated.

EXPERIMENTAL

Anionic maghemite nanoparticles

Negatively charged superparamagnetic nanocrystals of maghemite (γ-Fe_2O_3) were chemically synthesized according to Massart's method (29). The stability of the colloidal suspension was ensured by electrostatic repulsion between nanoparticles bearing citrate ligands with unbound carboxylate groups (COO^-). The nanoparticles have a ferrimagnetic core of maghemite with a mean diameter of 8 nm, carrying an effective magnetic moment $m_{eff} = M_S V$, where $M_S = 3.1 \times 10^5$ A/m^2 is the saturation magnetization of maghemite and V the particle volume. They exhibit superparamagnetic behaviour and no remnant magnetization.

Cell culture and magnetic labelling

Magnetic labelling was applied to HeLa ovarian tumour cells grown at 37°C with 5% CO_2 in Dulbecco's modified Eagle's medium (DMEM, Gibco, Invitrogen Corporation) supplemented with 10% heat-inactivated fetal calf serum, 50 U/ml penicillin, 40 μg/ml streptomycin and 0.3 mg/ml L-glutamine. HeLa cells were incubated for 60 min at 37°C with the magnetic nanoparticles AMNP at iron concentrations [Fe] of 0.15, 0.3, 0.6, 1, 2.5 and 5 mM in RPMI 1640 medium (Gibco) supplemented with 5 mM citrate sodium, followed by a 90 min chase in RPMI 1640 medium. AMNP flocculates in DMEM, but they are stable in RPMI supplemented with 5 mM citrate, so we used this medium for cell labelling.

Quantification of cellular magnetic load

Iron uptake by HeLa cells was quantified with a magnetophoresis assay as described elsewhere (30). Briefly, magnetophoresis consists of measuring the velocity acquired by magnetic cells in suspension, submitted to a magnetic field gradient ($B = 174$ mT, $dB/dz = 18.5$ mT/mm). In steady-state conditions, cell velocity is deduced from the balance between magnetic force (proportional to the cell magnetic moment in field B or equivalent to the iron mass per cell) and the friction force (proportional to cell velocity). The displacement of 50–100 cells was tracked by videomicroscopy in each labelling condition. Cell velocity and mean iron mass per cell were deduced as described in Wilhelm *et al.*(30).

Agarose gel preparation

Agarose phantoms of dispersed labelled cells were prepared as follows. After labelling and washing with 0.1 M cacodylate buffer, the cells were fixed for 1 h at 4°C in 2% glutaraldehyde in 0.1 M cacodylate buffer and washed again with cacodylate buffer. Cells were fixed for better stability of the sample. Cell pellets containing known numbers of labelled and unlabelled cells were gently mixed with 200 or 300 μl of low-melting-point 0.3% agarose gel at 40°C. Two series were prepared. The 'cell density' series consisted of a total of 10^7 HeLa cells in 300 μl of agarose with percentages of labelled cells (iron mass per cell $= 2.5 \pm 0.4$ pg) ranging from 0.01 to 1% (10^3–10^5 labelled cells). The 'labelling series' was composed of 200 μl of agarose gel containing 500 HeLa cells labelled with extracellular iron concentrations ranging from 0.15 to 5 mM.

Magnetization curve of labelled cells

The magnetization curve of 10^7 magnetically labelled HeLa cells (1 h of incubation at [Fe] = 5 mM, iron mass per cell $= 5.6 \pm 1.6$ pg) dispersed in 300 μl of agarose gel was measured as a function of magnetic field using a superconducting interference device (SQUID).

MRI measurement

High-resolution 9.4 T MRI was performed using a vertical wide-bore spectrometer (Inova, Varian), with a 2 T/m gradient coil and a home-built cylindrical coil 8 mm in diameter. MR images of labelled HeLa cells in agarose gel were acquired with gradient echo sequences. In all experiments the repetition time was 200 ms and the flip angle was equal to the Ernst angle calculated from the relaxation time of the sample without labelled cells. A two-dimensional gradient echo sequence (GE) was used for the first experiment on the cell density series, with an echo time of 3 ms, a slice thickness of 125 μm, a field of view of 6×6 mm and a 128×128 acquisition matrix. Zero-filling in each dimension led to an in-plane resolution of 23.5 μm^2. Labelled cells were counted in successive virtual slices extracted from a three-dimensional experiment recorded with an echo time of 3 ms, a field of view of $6 \times 6 \times 14.8$ mm and a $128 \times 128 \times 256$ acquisition matrix. With one accumulation per increment, the required experimental time was 1 h 50 min. Zero-filling applied in two directions resulted in a $256 \times 256 \times 256$ matrix and in a spatial resolution of $23.5 \times 23.5 \times 59$ μm.

Spin echo (SE) multislice sequences were used to measure the relaxation times of single HeLa cells (iron mass per cell $= 5.6 \pm 1.6$ pg). The two-dimensional sequence used a thickness of 250 μm, a field of view

DOI: 10.1002/cmmi

of 5×5 mm and an acquisition matrix of 128×128. The repetition time was 10 s. For T_2 measurements, echo times of 20, 40, 60, 80, 100, 200 and 500 ms were used. For T_1 measurement, an inversion recovery sequence was used with an echo time of 10 ms and recovery times of 20, 50, 100, 500, 1000, 2000 and 5000 ms.

For single HeLa cell imaging as a function of the intracellular iron mass and echo time, the echo time was varied from 2 to 30 ms in three-dimensional gradient echo experiments. The field of view was $5 \times 5 \times 5.5$ mm and the matrix $128 \times 128 \times 128$, giving a spatial resolution of $39 \times 39 \times 43$ μm, approximated in the text as 40 μm^3. The signal loss relative to the agarose gel was defined as $\Delta IS/IS_g = (IS_g - IS)/IS_g$, where IS_g is the mean signal intensity of the agarose gel (far from labelled cells) and IS is the signal intensity of the volume of interest. To investigate the effect of resolution, we first imaged the same sample with different voxel sizes. We have shown for one intracellular iron concentration that the values of the $\Delta IS/IS$ ratios for a given volume of interest (VOI) were similar (by taking in account the measurements errors) by using a resolution corresponding to this VOI or by averaging several voxels in order to obtain the size of the VOI, if the signal (of the agarose gel)-to-noise ratios were the same. Thus, the effect of resolution was studied in three-dimensional experiments with a resolution of 40 μm^3, by averaging several 40 μm^3 voxels in order to obtain volumes of 120, 200 and 280 μm^3, respectively. For each measurement, as a function of the echo time, cell iron mass or voxel size, the relative signal losses were averaged for 10 different cells. Images were analysed with WIN-MRI® software (Bruker Spectrospin, Wissembourg, France).

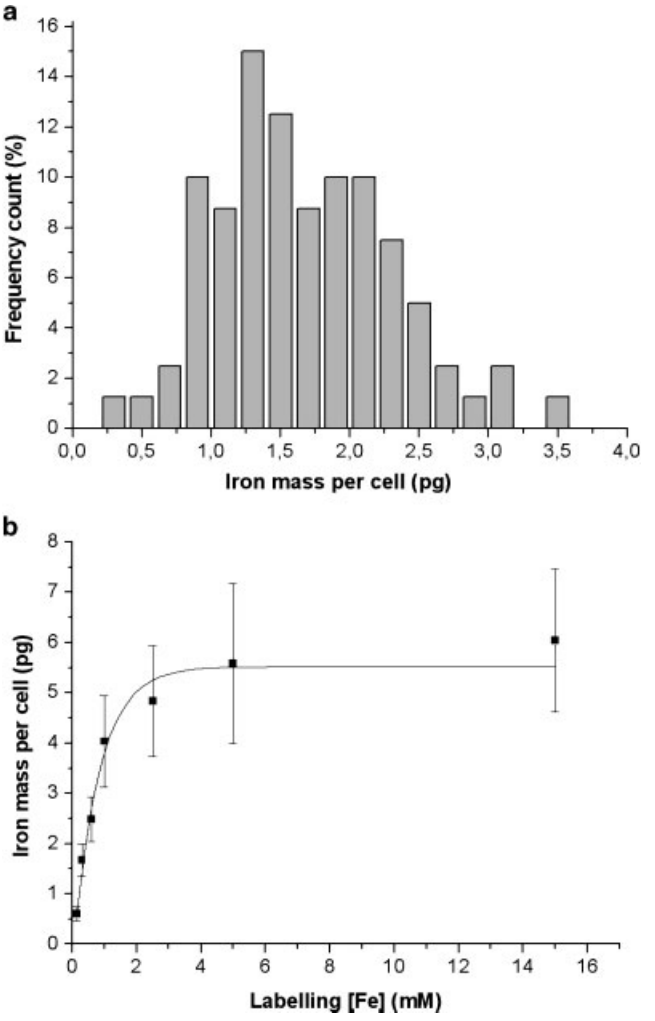

Figure 1. Quantification of cell iron load by magnetophoresis. (a) Distribution of iron mass per cell for a cell population ($n = 100$) labelled with an extracellular iron concentration [Fe] = 0.3 mM (1 h incubation at 37°C, 90 min chase). (b) Mean iron mass per cell (in pg) as a function of the extracellular iron concentration (1 h incubation at 37°C, 90 min chase). Bars represent the standard deviation determined from the whole distribution of iron mass for each labelling condition. Note that iron uptake reaches a plateau at [Fe] > 5 mM.

RESULTS

Magnetization of labelled cells

As magnetophoretic mobility was measured for individual cells, magnetophoresis provides the iron load distribution for the entire cell population. Figure 1(a) shows a typical histogram of particle uptake by HeLa cells (extracellular iron concentration [Fe] = 0.3 mM), while Fig. 1(b) shows the mean iron load as a function of the extracellular iron concentration used for the labelling procedure. As discussed in Wilhelm *et al.* (10), iron uptake reaches a plateau as the extracellular iron concentration (or incubation time, data not shown) is increased.

The magnetization of HeLa cells, normalized to its saturation value, is shown in Fig. 2 as a function of the magnetic field up to 5 T. The magnetization behaviour of labelled cells was similar to that of the maghemite nanoparticles in colloidal suspension. In particular, magnetization reached 95% of its saturation value at 1.5 T and was fully saturated at 5 T. Magnetically labelled cells, like maghemite nanoparticles, showed superparamagnetic properties with no remnant magnetization.

High resolution 9.4 T imaging

Single cell detection. Figure 3(a) and (b) shows slices of agarose gels imaged at 9.4 T using a gradient echo sequence (slice thickness 125 μm, sample volume 300 μl) containing labelled cells concentrations of respectively 330 and 3.3 cells/μl The slice volume was 2.46 μl, and each slice contained an average of respectively 817 and 8.17 labelled cells. A highly heterogeneous signal pattern was obtained with the slice containing an average of

DOI: 10.1002/cmmi

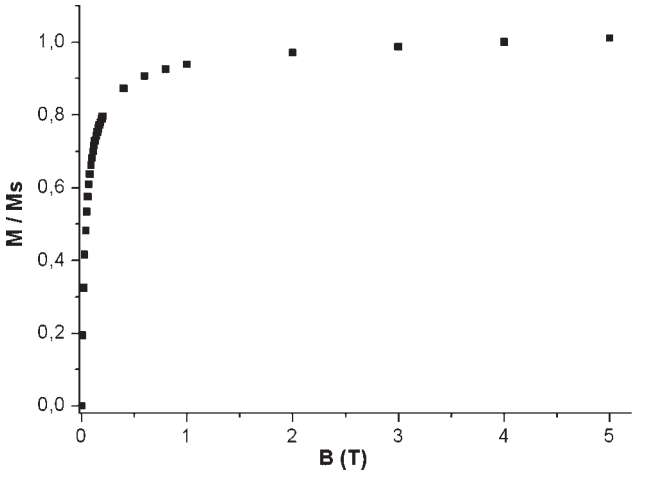

Figure 2. Magnetization *M* (normalized to the saturation magnetization *Ms*) as a function of the magnetic field B of magnetically labelled cells (iron mass per cell = 5.6 ± 1.6 pg). Magnetized cells show superparamagnetic behaviour, with magnetization saturating above 2 T and no remnant magnetization.

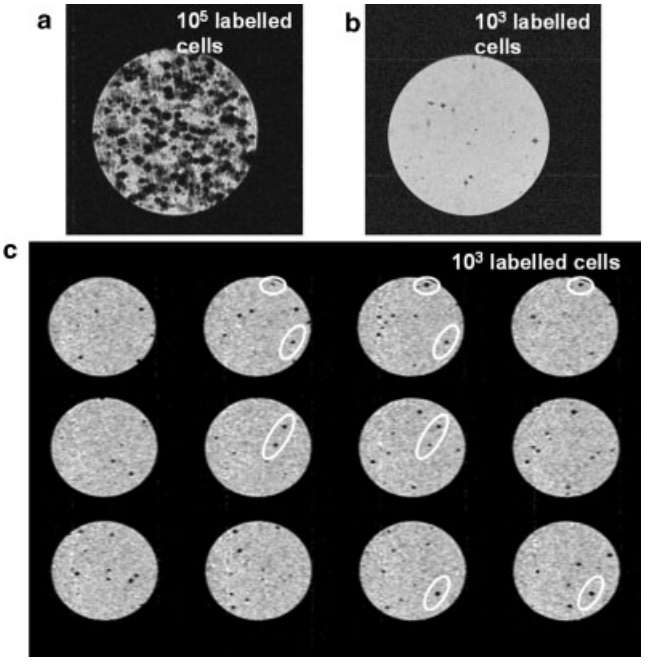

Figure 3. Detection of single cells with high-resolution GE 9.4 T MRI (in-plane resolution 23.5 × 23.5 μm, *TE* = 3 ms, *TR* = 200 ms, iron mass per cell = 2.5 ± 0.4 pg, gel volume = 300 μl). (a, b) Slices of agarose gel containing on average 817 (a) and 8.17 (b) labelled cells, respectively. Slice thickness is 125 μm. (c) Adjacent slices of gel containing statistically 3–4 labelled cells. Slice thickness is 59 μm and slice volume 1.14 μl. Note that a given signal void generally spans two successive slices. Assuming that the same cell appears on two slices, the observed number of signal voids per slice is consistent with the detection of individual cells.

817 labelled cells [Fig. 3(a)], whereas isolated dark spots were found on slices containing eight labelled cells on average [Fig. 3(b)].

Successive 59 μm-thick slices of this sample are shown in Fig. 3(c). Isolated dark points were easily detectable, and could be counted by taking in account the fact that a given signal void could span two adjacent slices. This counting was made over a volume of 25 μl corresponding to 22 slices, and gave 96 spots, which corresponded to 3.8 spots/μl on average.

The correlation between dark spots and cell numbers, together with the focal nature of the signal losses, indicated that mainly individual cells were detected, appearing as signal voids much larger than their actual size.

MR imaging of single cells

Relaxation times T_1 and T_2 around a single magnetic cell. Figure 4 shows the comparison between gradient echo (GE) and spin echo (SE) sequences (*TE* = 15 ms) for tracking an individual labelled cell: a magnetic cell was readily detected with the GE sequence, but was hardly visible on the SE image. Local modifications of proton relaxation times T_1 and T_2 due to cell magnetization (iron mass = 5.6 ± 1.6 pg) were then investigated. T_1 and T_2 were 95 and 83% of the agarose gel values in the central voxel containing the cell and returned to 100% in surrounding voxels. Thus, a single labelled cell had only a minor and very local effect on relaxation times T_1 and T_2, which explained the spin echo not being suitable to detect isolated labelled cells. Gradient echo sequences with T_2^* weighting were used in the rest of the study.

High-resolution (40 μm) GE sequence: echo time effect. We then investigated the effects of the echo time and cellular iron load on the cell image for a three-dimensional gradient echo sequence with voxel size

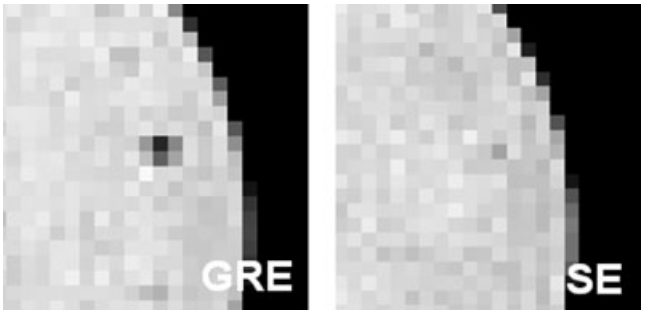

Figure 4. Detection of single cells with high-resolution 9.4 T MRI: SE vs GE sequences. Images of the same labelled cell acquired with a gradient echo sequence (left) and a spin echo sequence (right) at an echo time of 15 ms. The labelled cell is barely detectable on the SE image. The voxel size was 40 μm^3 and the iron mass per cell = 5.6 ± 1.6 pg.

DOI: 10.1002/cmmi

40 μm^3. As shown in Fig. 5(a), cell contrast spread spatially as the echo time increased. The apparent MR volume of each labelled cell was determined by counting the number of voxels whose signal loss $\Delta IS/IS_g$ was higher than $IS_g–IS_{gmin}/IS_g$, with IS_{gmin} the minimum intensity of the gel. The measurements were carried out on 10 cells for each intracellular iron mass. These apparent volume values are reported in Fig. 5(b) as a function of the echo time and for different per-cell iron masses. Even at 5 ms, the apparent cell volume, between $5 \times 40\ \mu m^3$ and $8 \times 40\ \mu m^3$, was much larger than the actual size (the diameter of a HeLa cell is about 20 μm). The increase in the apparent volume with the echo time was linear. By contrast, a 10-fold variation in cellular iron load or the equivalent cell magnetization had only a moderate influence on the apparent size of the cell. The spatial profile of relative signal loss $\Delta IS/IS_g$ is represented in Fig. 6 as a function of the distance d from the central voxel, for various echo times (cellular iron load = 2.5 ± 0.4 pg). Cell contrast spread by up to 120 μm from the central voxel, and the intensity profile broadened with increasing echo times.

Single cell detection with GE sequences: effect of resolution. To examine the effect of resolution on single cell detectability with 9.4 T GE sequences, the voxel size was varied from 40 to 280 μm^3. Figure 7 shows the relative signal loss in the central voxel (containing the cell) as a function of the voxel volume and for different echo times. The signal loss fell markedly with increasing voxel size, and was less than 10% at a 280 μm^3 resolution. Thus, voxel sizes larger than 280 μm^3 are unsuitable for single cell detection.

The echo time dependency of the different resolutions is clearly seen in Fig. 8. The relative signal loss in the central voxel increased with the echo time. Signal loss

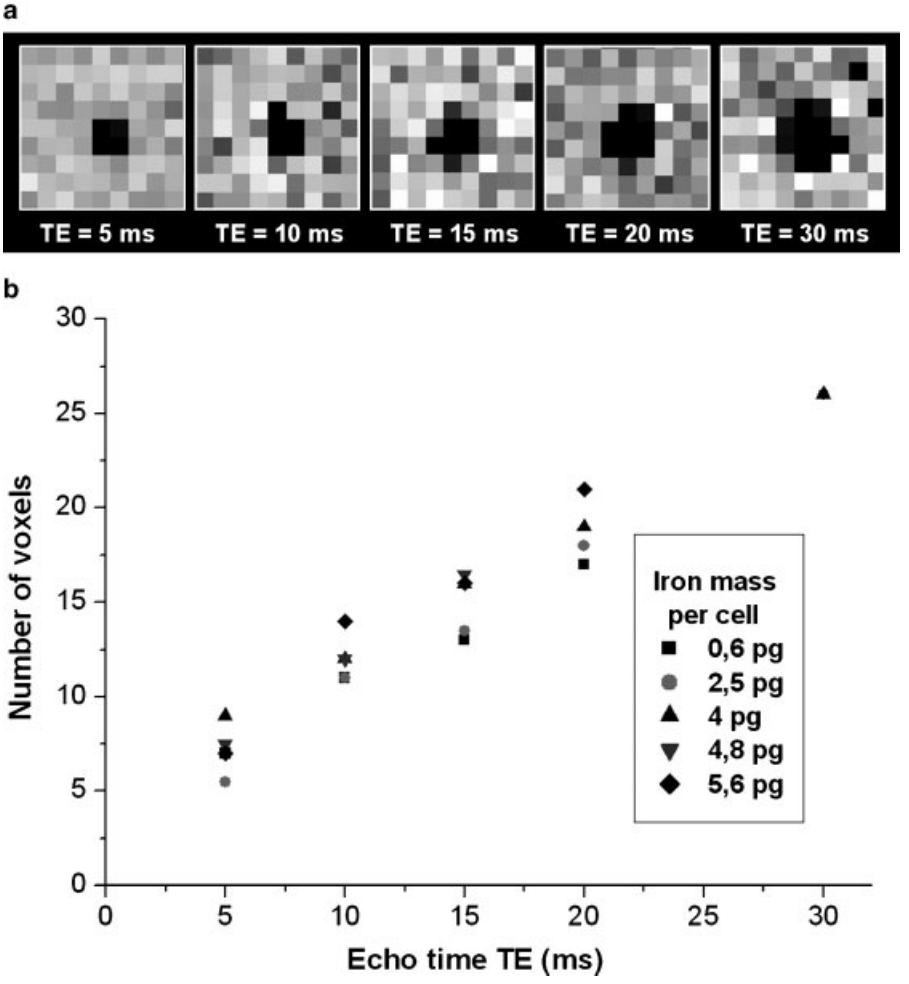

Figure 5. Influence of the echo time (high-resolution three-dimensional GE 9.4 T MRI). (a) The same labelled cell was imaged with different echo times. The cell contrast spread spatially with increasing echo times. The voxel size was 40 μm^3 and the iron mass per cell 5.6 ± 1.6 pg. (b) Number of voxels 40 μm^3 substantially affected by the cell magnetization (i.e. with relative signal loss >38%) as a function of the echo time and at different per-cell iron masses. The apparent size of the cell is much larger than its actual size and increases linearly with the echo time. The iron mass per cell has a more moderate influence on the apparent size of the cell.

DOI: 10.1002/cmmi

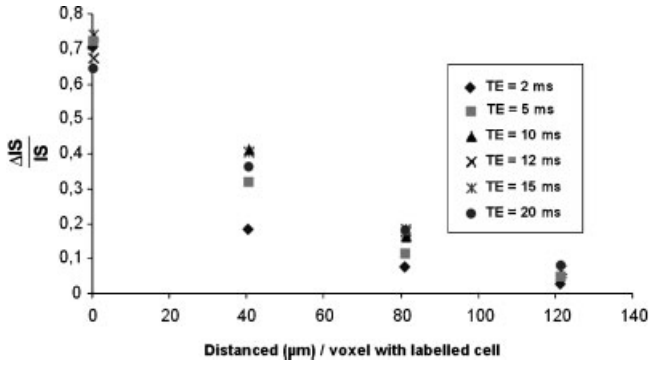

Figure 6. Cell signal profile (high-resolution three-dimensional GE 9.4 T MRI). Relative signal loss as a function of the distance from the voxel containing the labelled cell at different echo times. The voxel size is 40 μm^3 and the iron mass per cell 2.5 ± 0.4 pg. The cell contrast spreads up to 120 μm from the cell centre. The larger the echo time, the broader the signal profile.

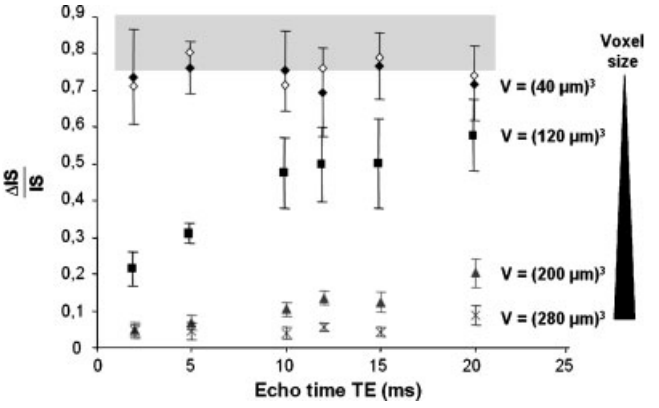

Figure 8. Combined influence of the echo time and voxel size on the relative signal loss in the voxel containing the cell (three-dimensional GE 9.4 T MRI, iron mass per cell = 2.5 ± 0.4 pg). The signal loss increases with increasing echo times and with decreasing voxel sizes. A labelled cell will be detectable if it induces a signal loss that exceeds the intrinsic signal fluctuations of the gel for a given voxel size. For resolutions of 280 and 200 μm^3, the background gel signal fluctuations are 5 and 6%, respectively, so that an echo time larger than 20 and 10 ms, respectively, will be necessary to detect an individual cell. For resolutions of 120 and 40 μm^3, the gel fluctuations (7.5 and 38%) are well below the relative signal loss, so that echo times as short as 2 ms can be used to detect single labelled cells. For a voxel size of 40 μm^3, the signal loss reaches the maximum value corresponding to a signal reduced to the noise level, whatever the echo time or cell iron load [iron mass of 0.6 pg (open diamond) or 2.5 pg (solid diamond)]. At high resolution, the contrast effect of the cell is saturating. The noise level is indicated in the figure by the grey rectangle.

was particularly sensitive to changes in the echo time at 120 μm^3 resolution (the relative signal loss varied linearly from 20 to 57%). At this resolution (Fig. 9), signal loss also increased with the iron mass per cell, but to a lesser extent than with the echo time. At lower resolutions the signal loss did not exceed 20% for $TE = 20$ ms.

In contrast, at the highest resolution 40 μm^3, for an intracellular iron mass between 0.6 and 5.6 pg, and when the echo time varied from 3 to 30 ms, signal loss depended neither on the echo time nor on the iron mass per cell: it saturated to the maximum value corresponding to the value $(IS_g - N)/IS_g$ calculated from the noise level N. At high resolution, the dephasing effect of the labelled cell completely cancelled the proton magnetization of the central voxel, even for cells with iron masses as low as 0.6 pg and for short echo times.

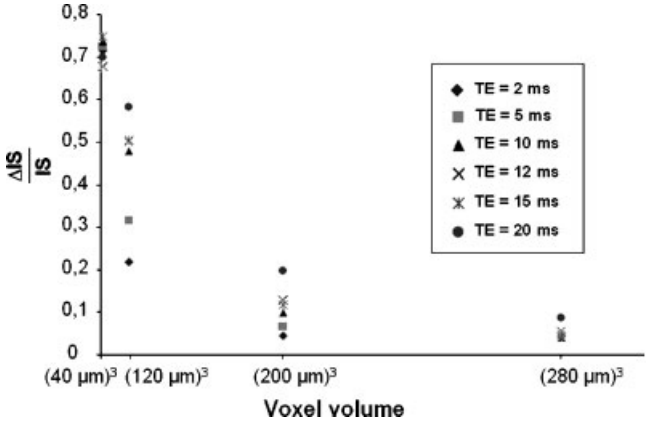

Figure 7. Effect of resolution (three-dimensional GE 9.4 T MRI). Relative signal loss in the voxel containing the cell as a function of voxel size and for different echo times. The iron mass per cell is 2.5 ± 0.4 pg. The signal loss falls drastically with increasing voxel size. At the highest resolution (40 μm^3), the signal loss is maximum whatever the echo time. For lower resolutions, the signal loss is clearly enhanced with the echo time. For voxel sizes above 280 μm^3, the signal loss falls to less than 10% and labelled cells are barely visible.

To determine a single cell detection threshold, one must compare the relative signal loss produced by the cell with the signal fluctuations of the surrounding agarose gel. The signal loss must be larger than the value $IS_g - IS_{gmin}/IS_g$, where IS_{gmin} is the minimum intensity of the gel. For resolutions of 280 and 200 μm^3, gel signal fluctuations were 5 and 6%, respectively. Based on changes in the cell-induced signal loss with the echo time, echo times longer than 20 and 10 ms, respectively, would be necessary for single cell detection. By contrast, at resolutions of 120 and 40 μm^3, gel signal fluctuations (7.5 and 38%, respectively) were well below the cell signal loss, whatever the experimental echo time. Within the limits of voxel sizes smaller than 120 μm^3, echo times as short as 2 ms can be used to detect individual labelled cells.

DISCUSSION

The challenge of MRI cell detection with even higher resolution has been motivated by the recent progress in

DOI: 10.1002/cmmi

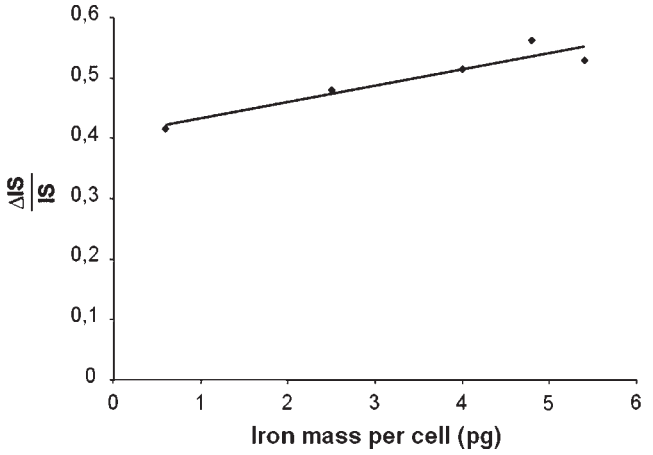

Figure 9. Influence of iron mass per cell on the relative signal loss in the central voxel. Voxel size = 120 μm^3 and $TE = 10$ ms. The signal loss varies linearly with iron mass per cell, but the variation is small compared with the echo time effect at the same resolution.

cell-based therapy. After iron oxide nanoparticle labelling, high-resolution MRI can detect single cells *in vitro* (21,22) and also in mouse liver (27) and mouse brain (28). Even if these MR images were acquired at low resolution compared with the size of the cell, the presence of a labelled cell within an imaging voxel affects the signal of the voxel of interest and, possibly, surrounding voxels. Non-ambiguous identification of labelled cells in a signal pattern may suffer from signal loss due to many other factors. In particular, high magnetic field strength, by enhancing diamagnetic proton magnetization, emphasizes artefacts near magnetic susceptibility interfaces. Hence, it is useful to analyse local effects of single labelled cells on MR sequence parameters. High-field MRI is suitable for single cell detection because of the additional endogenous signal and the higher spatial resolution that results from it (31). Indeed, sample nuclear magnetization increases linearly with the magnetic field. The magnetization of exogenous ferromagnetic contrast agents such as iron oxide nanoparticles saturates at relatively low field strengths, because the permanent magnetic moment of each grain is blocked in the direction of the external field, preventing orientational thermal fluctuations. Maghemite nanoparticles of typical diameter 8 nm reach 95% of their saturation magnetization at 1.5 T. As shown in Fig. 2, cells labelled with these nanoparticles exhibit the same magnetization curve as the same isolated nanoparticles in colloidal suspension.

Contrast around a single magnetic cell is essentially governed by the acceleration of water relaxation due to magnetic field gradients generated by cell magnetization (32,33). Three characteristic times scales determine the relevant regime of relaxation. The first characteristic time τ_0 is the time taken for a proton to be dephased by one radian when submitted to the rms angular frequency shift $\Delta\omega$ due to the field created by the magnetized cell. It is inversely proportional to the amplitude of the local magnetic field, which depends on the distance from the cell centre and on the direction relative to the static field. Second, the diffusion time τ_D is the time taken for water molecules to diffuse through a distance r, in any direction. It increases with the square of this distance as $\tau_D = r^2/D$, where D is the water diffusion coefficient. The third time is the experimental echo time TE, which is the time required for free relaxation to occur before the refocusing pulse of spin echo sequences.

The diffusion time τ_D, during which a diffusing proton remains under the influence of the magnetic inhomogeneity, defines two regimes of nuclear relaxation. If $\tau_D \ll \tau_0$, the motional averaging condition is satisfied. This is the case, for example, for a dispersed solution of maghemite nanoparticles, as r is the particle diameter (about 10 nm). In contrast, if $\tau_D \gg \tau_0$, proton magnetization is substantially relaxed by the local field inhomogeneity before the protons escape from the region of field inhomogeneity by diffusion. In extreme conditions, the so-called static dephasing regime (SDR) (20,33,34) refers to the dephasing of motionless protons in a non-uniform field. It places an absolute limit on the relaxation rate—a limit reached in the absence of a refocusing pulse. The static dephasing regime remains valid if the motion is slow enough to satisfy the condition $\Delta\omega\tau_D > 1$. This limit requires strong magnetization and slow diffusion in the region of high field inhomogeneities. Magnetically labelled cells meet these requirements. The time τ_D taken by a water molecule to diffuse across a cell diameter (20 μm) is about 170 ms, and exceeds 1 s over the voxel size. The magnetized cell can be approximated by a uniformly magnetized sphere, generating a pure dipole field decreasing as $1/r^3$, where r is the distance from the cell centre. A cell with magnetic moment $m = 4.9 \times 10^{-13}$ A m^2 (corresponding to 5 pg of iron) produces a magnetic field with z component (along the MR static field) B_z ($r = 10\,\mu m$) $= 10^{-4}$ T ($\tau_0 = 0.037$ ms) at its surface and B_z ($r = 50\,\mu m$) $= 8 \times 10^{-7}$ T ($\tau_0 =$ 4.7 ms) 50 μm from its centre. As a consequence, the condition of validity of the static dephasing regime, $\Delta\omega\tau_D > 1$, is fulfilled in a region extending 300 μm around the cell. In this context, it is easy to explain the lack of local T_2 effect with spin echo sequences (Fig. 4). As diffusion is slow compared with the relaxation due to cell susceptibility, the field inhomogeneity can be considered as static by the proton, giving rise to a pure T_2^* effect with no contribution to T_2 relaxation. The refocusing pulses (whatever $\tau_D > TE > \tau_0$) reconstruct the nuclear magnetization. In this limit of static dephasing regime, the local R_2 enhancement due to cell magnetization approaches zero, as observed in our experiments (Fig. 4) and spin echo sequences are poorly sensitive to local cell magnetization. In contrast, FID or gradient echo acquisition does not involve refocusing pulses, so these sequences are fully sensitive to the relaxation process induced by strongly magnetized micrometric perturbers.

DOI: 10.1002/cmmi

Thus, in agreement with the experimental evidence, gradient echo acquisition is necessary for accurate detection of single magnetic cells.

Gradient echo sequences are directly sensitive to local field inhomogeneities, and the echo time represents the time available for proton magnetization to be dephased before MR detection. For protons in the same voxel, the frequency spread due to the local field gradient leads to an accumulation of different spin phases, resulting in signal loss that increases with time. Thus, as demonstrated in Figs 5 and 6, the spatial extension of detectable signal loss, defined here as the apparent volume of the cell, is amplified with the echo time. At high resolution, 40 μm^3, we found that the signal loss saturated in the voxel containing the cell, being independent of both the echo time and cell magnetization. By contrast, the echo time dependency was detectable in neighbouring voxels (typically up to 100 μm from the cell centre). Beyond, the signal tends towards the agarose gel signal. This spatial dependency of signal loss is consistent with the $1/r^3$ decline in the dipolar field induced by the magnetic cell.

As expected from the very sharp signal profile around a magnetic cell, the choice of resolution appears crucial for single cell detection. Indeed, the signal loss in the voxel containing the cell falls drastically with increasing voxel size. For voxel sizes larger than 200 μm, the cell-induced signal loss does not exceed 20%, so that the intrinsic signal variation of the background medium determines the discrimination of the presence of a labelled cell. For a homogeneous medium such as agarose gel, the intrinsic signal variation reaches 6% at a resolution of 200 μm, and does not vary significantly with the echo time. Thus, given the linear increase in signal loss with the echo time (Fig. 8), the detection of an individual cell would require the use of a relatively long echo time (above 10 ms). At 280 μm resolution, single cell detection would require an echo time longer 20 ms. In practice, the detection threshold is determined by at least two interdependent parameters—echo time and resolution—and, to a lesser extent, iron mass per cell. For higher resolutions, such as 120 and 40 μm^3, the intrinsic variations of the gel signal are minimal compared with the cell-induced signal loss, even for echo times as short as 2 ms. Hence, short echo times (allowing minimal diamagnetic susceptibility effect on background medium), together with high resolution, are appropriate conditions for discrimination of individual magnetic cells, both *in vitro* and *in vivo*.

It is interesting to note that a 10-fold variation in cell magnetization resulted in only a small change in signal loss (40–55%), observable only at intermediate resolution (120 μm^3). Moreover, at higher resolution (40 μm^3), the cell signal falls to the noise level whatever the echo time and whatever the iron mass per cell between 0.6 and 5.6 pg.

On one part, intercellular variability of iron load [Fig. 1(a)] or number and position of cell within the voxel may explain the weak dependency of signal loss on cell magnetization. On the other part, at low voxel volume, 40 μm^3, the relative signal loss in the central voxel saturates whatever the cell magnetization and for echo times from 2 to 20 ms. This result has important implications for the feasibility of *in vivo* and *ex vivo* cell tracking.

Relevance to single cell detection *in vivo* and *ex vivo*

One major consideration for cell tracking is that cells transplanted *in vivo* may undergo several divisions. It has been shown that magnetic nanoparticles were equally distributed among daughter cells during 14 days of cell culture (15). However saturation of signal loss may enable cell detection even after several divisions.

Another obstacle for single cell detection *in vivo* is the intrinsic variation of susceptibility in the tissue (35), whose relaxing effect is emphasized by increasing magnetic fields and echo times. As demonstrated here, short echo times can be used, when combined with high resolution imaging, to detect single cells with relatively low iron loads. Thus, the use of short echo times would minimize non-specific signal losses without compromising discrimination of specific cells in an organ.

High-resolution MRI associated with cellular magnetic labelling (36) may be complementary to histology. As shown in Shapiro *et al.*(27) and Heyn *et al*. (28), images of single cells or small clusters of cells can be superimposed on optical micrographs. Even if the apparent size of labelled cells exceeds their actual size by at least a factor of 2, MR offers the advantages of non-destructive three-dimensional exploration of organs '*ex vivo*'. Moreover, with resolutions of the order of 40 μm^3, MRI may be more sensitive to cells with subpicogram iron loads than with conventional Prussian blue coloration (14). Finally, magnetic labelling of cells can be combined with specific *in vivo* or *ex vivo* optical labelling, offering the possibility of multimodal imaging, which would be helpful for analysing the precise fate of injected therapeutic cells.

CONCLUSION

We investigated the detection of single cells labelled with anionic iron oxide nanoparticles in a 9.4 T MRI device. High resolution GE sequences detected individual labelled cells, whereas SE sequences were poorly sensitive to local cell magnetization. The signal loss produced by labelled cells enhanced and spread spatially with increasing echo times on GE sequences, and diminished rapidly with increasing voxel size. In the high resolution limit, the signal loss saturates whatever the echo time and cellular iron load, permitting the

DOI: 10.1002/cmmi

detection of cells with subpicogram iron masses. This *in vitro* study provides the basis for experiments aimed at single cell detection with GE sequences *in vivo*.

Acknowledgements

We thank Professor J. Bittoun for scientific advises, Professor J.-C. Bacri, Professor O. Clément and J.-P. Fortin-Ripoche for helpful discussions, and Dr C. Ménager for providing us with the citrated maghemite nanoparticles. This work was supported by grants from CNRS and the French Ministry of Research (ACI Nanoscience et Nanotechnologie NR0145 and Programme Interdisciplinaire Imagerie du Petit Animal).

P. Smirnov and F. Gazeau contributed equally to this work.

REFERENCES

1. Bulte JW, Kraitchman DL. Iron oxide MR contrast agents for molecular and cellular imaging. *NMR Biomed.* 2004; **17** (7): 484–499.
2. Bulte JW, Zhang S, van Gelderen P, Herynek V, Jordan EK, Duncan ID, Frank JA. Neurotransplantation of magnetically labelled oligodendrocyte progenitors: magnetic resonance tracking of cell migration and myelination. *Proc. Natl Acad. Sci. USA* 1999; **96** (26): 15256–15261.
3. Bulte JW, Douglas T, Witwer B, Zhang SC, Strable E, Lewis BK, Zywicke H, Miller B, van Gelderen P, Moskowitz BM, Duncan ID, Frank JA. Magnetodendrimers allow endosomal magnetic labelling and *in vivo* tracking of stem cells. *Nat. Biotechnol.* 2001; **19** (12): 1141–1147.
4. Hoehn M, Kustermann E, Blunk J, Wiedermann D, Trapp T, Wecker S, Focking M, Arnold H, Hescheler J, Fleischmann BK, Schwindt W, Buhrle C. Monitoring of implanted stem cell migration *in vivo*: a highly resolved *in vivo* magnetic resonance imaging investigation of experimental stroke in rat. *Proc. Natl Acad. Sci. USA* 2002; **99** (25): 16267–16272.
5. Kircher MF, Allport JR, Graves EE, Love V, Josephson L, Lichtman AH, Weissleder R. *In vivo* high resolution three-dimensional imaging of antigen-specific cytotoxic T-lymphocyte trafficking to tumors. *Cancer Res.* 2003; **63** (20): 6838–6846.
6. Lewin M, Carlesso N, Tung CH, Tang XW, Cory D, Scadden DT, Weissleder R. Tat peptide-derivatized magnetic nanoparticles allow *in vivo* tracking and recovery of progenitor cells. *Nat. Biotechnol.* 2000; **18** (4): 410–414.
7. Modo M, Mellodew K, Cash D, Fraser SE, Meade TJ, Price J, Williams SC. Mapping transplanted stem cell migration after a stroke: a serial, *in vivo* magnetic resonance imaging study. *Neuroimage* 2004; **21** (1): 311–317.
8. de Vries IJ, Lesterhuis WJ, Barentsz JO, Verdijk P, van Krieken JH, Boerman OC, Oyen WJ, Bonenkamp JJ, Boezeman JB, Adema GJ, Bulte JW, Scheenen TW, Punt CJ, Heerschap A, Figdor CG. Magnetic resonance tracking of dendritic cells in melanoma patients for monitoring of cellular therapy. *Nat. Biotechnol.* 2005; **23** (11): 1407–1413.
9. Anderson SA, Shukaliak-Quandt J, Jordan EK, Arbab AS, Martin R, McFarland H, Frank JA. Magnetic resonance imaging of labelled T-cells in a mouse model of multiple sclerosis. *Ann. Neurol.* 2004; **55** (5): 654–659.
10. Wilhelm C, Gazeau F, Roger J, Pons JN, Bacri JC. Interaction of anionic superparamagnetic nanoparticles with cells: kinetic analyses of membrane adsorption and subsequent internalization. *Langmuir* 2002; **18**: 8148–8155.
11. Wilhelm C, Cebers A, Bacri JC, Gazeau F. Deformation of intracellular endosomes under a magnetic field. *Eur. Biophys. J.* 2003; **32** (7): 655–660.
12. Arbab AS, Bashaw LA, Miller BR, Jordan EK, Bulte JW, Frank JA. Intracytoplasmic tagging of cells with ferumoxides and transfection agent for cellular magnetic resonance imaging after cell transplantation: methods and techniques. *Transplantation* 2003; **76** (7): 1123–1130.
13. Naveau A, Smirnov P, Menager C, Gazeau F, Clement O, Lafont A, Gogly B. Phenotypic study of human gingival fibroblasts labeled with superparamagnetic anionic nanoparticles. *J. Periodontol.* 2006; **77** (2): 238–247.
14. Smirnov P, Lavergne E, Gazeau F, Lewin M, Doan B, Gillet B, Combadiere C, Combadiere B, Clement O. *In vivo* cellular imaging of lymphocytes trafficking by MRI: a tumor model approach for cell-based anticancer therapy. *Magn. Reson. Imag.* 2006 (in press).
15. Riviere C, Boudghene FP, Gazeau F, Roger J, Pons JN, Laissy JP, Allaire E, Michel JB, Letourneur D, Deux JF. Iron oxide nanoparticle-labelled rat smooth muscle cells: cardiac MR imaging for cell graft monitoring and quantitation. *Radiology* 2005; **235** (3): 959–967.
16. Smirnov P, Gazeau F, Lewin M, Bacri JC, Siauve N, Vayssettes C, Cuenod CA, Clement O. *In vivo* cellular imaging of magnetically labelled hybridomas in the spleen with a 1.5-T clinical MRI system. *Magn. Reson. Med.* 2004; **52** (1): 73–79.
17. Billotey C, Aspord C, Beuf O, Piaggio E, Gazeau F, Janier MF, Thivolet C. T-cell homing to the pancreas in autoimmune mouse models of diabetes: *in vivo* MR imaging. *Radiology* 2005; **236** (2): 579–587.
18. Moore A, Zhe Sun P, Cory D, Hogemann D, Weissleder R, Lipes MA. MRI of insulitis in autoimmune diabetes. *Magn. Reson. Med.* 2002; **47** (4): 751–758.
19. Billotey C, Wilhelm C, Devaud M, Bacri JC, Bittoun J, Gazeau F. Cell internalization of anionic maghemite nanoparticles: quantitative effect on magnetic resonance imaging. *Magn. Reson. Med.* 2003; **49** (4): 646–654.
20. Bowen CV, Zhang X, Saab G, Gareau PJ, Rutt BK. Application of the static dephasing regime theory to superparamagnetic iron-oxide loaded cells. *Magn. Reson. Med.* 2002; **48** (1): 52–61.
21. Dodd SJ, Williams M, Suhan JP, Williams DS, Koretsky AP, Ho C. Detection of single mammalian cells by high-resolution magnetic resonance imaging. *Biophys. J.* 1999; **76** (1 Pt 1): 103–109.
22. Foster-Gareau P, Heyn C, Alejski A, Rutt BK. Imaging single mammalian cells with a 1.5 T clinical MRI scanner. *Magn. Reson. Med.* 2003; **49** (5): 968–971.
23. Hinds KA, Hill JM, Shapiro EM, Laukkanen MO, Silva AC, Combs CA, Varney TR, Balaban RS, Koretsky AP, Dunbar CE. Highly efficient endosomal labelling of progenitor and stem cells with large magnetic particles allows magnetic resonance imaging of single cells. *Blood* 2003; **102** (3): 867–872.
24. Heyn C, Bowen CV, Rutt BK, Foster PJ. Detection threshold of single SPIO-labelled cells with FIESTA. *Magn. Reson. Med.* 2005; **53** (2): 312–320.
25. Shapiro EM, Skrtic S, Sharer K, Hill JM, Dunbar CE, Koretsky AP. MRI detection of single particles for cellular imaging. *Proc. Natl Acad. Sci. USA* 2004; **101** (30): 10901–10906.
26. Zhang Z, van den Bos EJ, Wielopolski PA, de Jong-Popijus M, Bernsen MR, Duncker DJ, Krestin GP. *In vitro* imaging of single living human umbilical vein endothelial cells with a clinical 3.0-T MRI scanner. *Magma* 2005; **18** (4): 175–185.
27. Shapiro EM, Sharer K, Skrtic S, Koretsky AP. *In vivo* detection of single cells by MRI. *Magn. Reson. Med.* 2006; **55** (2): 242–249.
28. Heyn C, Ronald JA, Mackenzie LT, MacDonald IC, Chambers AF, Rutt BK, Foster PJ. *In vivo* magnetic resonance imaging of single cells in mouse brain with optical validation. *Magn. Reson. Med.* 2006; **55** (1): 23–29.
29. Massart R. Preparation of aqueous magnetic liquids in alkaline and acidic media. *IEEE Trans. Magn.* 1981; **17**: 1247–1248.
30. Wilhelm C, Gazeau F, Bacri JC. Magnetophoresis and, ferromagnetic resonance of magnetically labelled cells. *Eur. Biophys. J.* 2002; **31** (2): 118–125.
31. Stroh A, Faber C, Neuberger T, Lorenz P, Sieland K, Jakob PM, Webb A, Pilgrimm H, Schober R, Pohl EE, Zimmer C. *In vivo* detection limits of magnetically labelled embryonic stem cells in the rat brain using high-field (17.6 T) magnetic resonance imaging. *Neuroimage* 2005; **24** (3): 635–645.

32. Gillis P, Koenig SH. Transverse relaxation of solvent protons induced by magnetized spheres: application to ferritin, erythrocytes, and magnetite. *Magn. Reson. Med.* 1987; **5** (4): 323–345.
33. Gillis P, Moiny F, Brooks RA. On *T*2-shortening by strongly magnetized spheres: a partial refocusing model. *Magn. Reson. Med.* 2002; **47** (2): 257–263.
34. Yablonskiy DA, Haacke EM. Theory of NMR signal behavior in magnetically inhomogeneous tissues: the static dephasing regime. *Magn. Reson. Med.* 1994; **32** (6): 749–763.
35. Shapiro EM, Skrtic S, Koretsky AP. Sizing it up: cellular MRI using micron-sized iron oxide particles. *Magn. Reson. Med.* 2005; **53** (2): 329–338.
36. Zhang Y, Kohler N, Zhang M. Surface modification of superparamagnetic magnetite nanoparticles and their intracellular uptake. *Biomaterials* 2002; **23** (7): 1553–1561.

DOI: 10.1002/cmmi